THE JOURNAL OF PHYSICAL CHEMISTRY B

Article

pubs.acs.org/JPCB

Temperature Dependence and Energetics of Single Ions at the Aqueous Liquid−Vapor Interface

Shuching Ou and Sandeep Patel*

Department of Chemistry and Biochemistry, University of Delaware, Newark, Delaware 19716, United States

Supporting Information

ABSTRACT: We investigate temperature-dependence of free energetics with two single halide anions, I^- and Cl^-, crossing the aqueous liquid−vapor interface through molecular dynamics simulations. The result shows that I^- has a modest surface stability of 0.5 kcal/mol at 300 K and the stability decreases as the temperature increases, indicating the surface adsorption process for the anion is entropically disfavored. In contrast, Cl^- shows no such surface state at all temperatures. Decomposition of free energetics reveals that water−water interactions provide a favorable enthalpic contribution, while the desolvation of ion induces an increase in free energy. Calculations of surface fluctuations demonstrate that I^- generates significantly greater interfacial fluctuations compared to Cl^-. The fluctuation is attributed to the malleability of the solvation shells, which allows for more long-ranged perturbations and solvent density redistribution induced by I^- as the anion approaches the liquid−vapor interface. The increase in temperature of the solvent enhances the inherent thermally excited fluctuations and consequently reduces the relative contribution from anion to surface fluctuations, which is consistent with the decrease in surface stability of I^-. Our results indicate a strong correlation with induced interfacial fluctuations and anion surface stability; moreover, resulting temperature dependent behavior of induced fluctuations suggests the possibility of a critical level of induced fluctuations associated with surface stability.

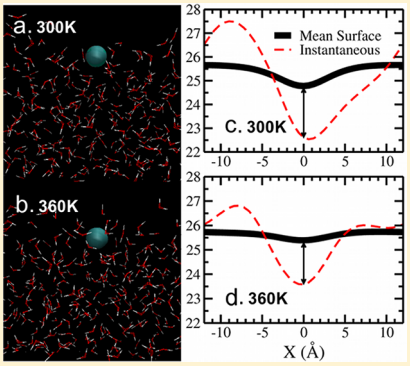

I. INTRODUCTION

Beginning with the theoretical/computational view of the stability of specific ions at aqueous liquid−vapor interfaces put forth in the work of Berkowitz et al,[1,2] Tobias and Jungwirth,[3−15] Dang and co-workers,[16−22] and recently more coarse-grained theories based on dielectric continuum,[23−25] the discussion of specific-ion effects,[16,17,19] particularly differential stabilities of halides at aqueous liquid−vapor interfaces and generally at hydrophobic interfaces, continues. The understanding of physical origins of differential stabilities of anions is of broad interest as specific-ion effects are implicated in processes ranging from protein denaturation, surface tension modulation, carbon nanomaterial self-association, and ion association with lipid bilayers and membranes.[26] Efforts to present unifying explanations of the molecular, thermodynamic, and structural underpinnings of these effects has garnered significant attention from theory and experiment, and continues to do so. We refer to a sampling of the vast literature.[13,15,24,26−40] In the context of differential stabilities of ions at the aqueous liquid−vapor interface, it is widely accepted that several factors conspire to give rise to interfacial stability in the case of the larger halides such as I^- and Br^-, and lack thereof in the case of smaller halides such as F^- and Cl^- (reflecting the reverse canonical Hofmeister series). Major molecular/atomic properties implicated are ion size, ion polarizability, ion hydration properties (free energy and entropy), ion charge density, and solvent polarizability and dipole moment.[41] Recently, the surface potential of the liquid vapor interface originating from classical point charge descriptions of molecular electrostatic distributions has been implicated as a major factor in interfacial ion partitioning.[42−47]

Affinity of ions to hydrophobic interfaces in a chemically specific manner has been documented experimentally as well. Rankin et al. addressed differences in interactions between halide anions F^- and I^- and *t*-butyl alcohol (TBA) in aqueous solution using Raman spectroscopy with multivariate curve resolution (Raman-MCR).[48] The authors demonstrated that, for 3 M NaI solutions, roughly 64% of *t*-butyl alcohol molecules are affected by I^- based on a red-shift of the CH stretch Raman frequency of about 5 cm^{-1} relative to *t*-butyl alcohol in pure water. Furthermore, computational modeling using EFP/MD and quantum mechanical QM/EFP1 methods showed that the alcohol interacts with I^- in the region of the alcohol headgroup (OH^-) and near the aliphatic CH_3 groups. Interestingly, the authors observed no experimental indication of Na^+ or F^- perturbations to the alcohol's vibrational modes. Recently, Otten et al.[49] used second harmonic generation (SHG) to probe surface adsorption thermodynamics for NaSCN (sodium thiocyanate) solutions, considering SCN^- as a prototypical chaotropic ion with unambiguous stability at the aqueous liquid−vapor interface. The authors demonstrated by fitting their SHG data to a Langmuir adsorption isotherm model that

Received: February 3, 2013
Revised: March 26, 2013

   dx.doi.org/10.1021/jp401243m | *J. Phys. Chem. B* XXXX, XXX, XXX−XXX

the inherent enthalpy and entropy of adsorption for SCN^- are negative, in keeping with earlier simulations[50] and experiment. The negative adsorption enthalpy was considered to challenge currently held theoretical views of the thermodynamic underpinnings of these ion behaviors. Zhang et al. examined the influence of 11 sodium salts on the stability of poly(*N*-isopropylacrylamide).[51,52] Kosmotropic anions were shown to polarize the water molecules hydrating the macromolecule, whereas the chaotropic anions directly interact with the macromolecule. The former of these mechanisms resulted in salting-out of the macromolecule, whereas the latter influenced salting-in.[51,52] Similar results were observed from molecular dynamics simulations of model systems. Heyda et al.[12] showed using extensive molecular dynamics simulations of *N*-methylacetamide (NMA) in the presence of monovalent cations and anions in water that the cations exhibit strong association with the carbonyl moiety of the peptide bond, while the anions do not interact with the amide group. Moreover, the larger anions, bromide and iodide, demonstrated preferential spatial correlation with the hydrophobic methyl group. This interaction was more evident in the simulations with polarizable force fields.

Finally, recent studies have illuminated the contributions of effects characteristic of hydrophobic hydration to halide interface propensity;[25,42,53] moreover, fluctuations of water–hydrophobe interfaces have been linked to differential interfacial stabilities. With the recent connection of surface stability of select inorganic anions (iodide, and partially charge iodide, for instance) to interfacial fluctuations and spatial correlations thereof,[49,54] there appears an intriguing mechanistic theme for ion-specific effects revolving around interfacial fluctuations induced by individual ions quite distant from the interface. This has broad implications in the context of discussing specific ion effects in a variety of circumstances. Thus, we also ask what differential influences single ions may have at distant interfaces.

Computational experiments measuring the reversible work (potential of mean force, PMF) for transferring single ions from bulk aqueous environment to the aqueous liquid–vapor interface have enjoyed a long history as a means to explore the origins of surface stability.[16,18,21] As mentioned above, to date, only one temperature dependence study on monovalent halides has been presented in the literature.[53] As mentioned in that work, the idea of negative adsorption entropy is independent of force field used to model the molecular components. This has also been demonstrated experimentally for NaSCN (as mentioned above). Thus, in this contribution, we first consider the temperature dependence of the potentials of mean force for single iodide and chloride anions in TIP4P-FQ water using classical umbrella sampling molecular dynamics simulations coupled with the weighted histogram analysis method (WHAM).[55] We then analyze local self- and cross-interaction (i.e., water–water and water–ion) energies underlying the observed potentials of mean force and temperature dependencies. Few studies in the literature have addressed the temperature dependence of single ion free energetics at the liquid–vapor interface, and we hope to compare and contrast the properties we observe with those discussed in earlier studies. We further consider solvent properties in the hydration shells of the two anions with the aim of comparing and contrasting radially dependent solvent properties such as water molecular dipole moment, water tetrahedrality, water–water interaction, and water–ion interaction energies; we hope to gain further insight into energetic and molecular structural origins of the differences in the surface stabilities of these two anions representing the neutral and chaotropic positions on the canonical Hofmeister series. These analyses will tie into recent work connecting local hydration properties and energetics of halide anions to surface propensity. Finally, we address aspects of the influence of the two anions on interface fluctuations in the spirit of Otten et al.[49]

This study is organized as follows. In section II we outline the methods, force fields, and related issues. We next present our results in section III, including the potential of mean force along with its decomposition (section IIIA) and L-V surface height fluctuations with the presence of single anion (section IIIB). We conclude in section IV.

II. METHODS

Molecular dynamics simulations were performed using the CHARMM package.[56] Simulations of liquid–vapor interfaces were performed in the NVT ensemble. Temperature was maintained at T = 280, 300, 320, 340, and 360 K using a Nosé-Hoover thermostat.[57] The simulation cell was rectangular with dimensions 24 Å × 24 Å × 100 Å, in which z is the direction normal to the liquid–vapor interface. A bulk slab consisting of 988 water molecules (represented by the polarizable TIP4P-FQ model[58]) and a single ion (Cl^-, I^-) was positioned in the center of the simulation cell, resulting in two liquid–vapor interfaces. A rigid water geometry is enforced using SHAKE[59] constraints. We employ polarizable TIP4P-FQ[58] water model and non-polarizable anions treated as charged Lennard–Jones spheres. Polarization of water is treated with a charge equilibration Hamiltonian:[60−63]

$$E_{\mathrm{elec}} = \sum_{i=1}^{N} (\chi_i) q_i + \frac{1}{2} \sum_{i=1}^{N} \eta_i {q_i}^2 + \frac{1}{2} \sum_{i \neq j}^{N} J_{ij} q_i q_j \qquad (1)$$

where χ_i and η_i may be associated with atomic electronegativities and hardnesses, respectively; the J_{ij} terms represent a parametrized molecular Coulomb integral between pairs of atoms. Components of the molecular polarizability tensor are related to the inverse of the hardness matrix (constructed from the values of η_i and J_{ij} above) as $\alpha_{\beta\gamma} = \mathbf{R}_\beta \mathbf{J}^{-1} \mathbf{R}_\gamma$ where $\mathbf{R}_\beta$ represents the β Cartesian components of the atomic position vector.[64]

The polarizable TIP4P-FQ water model employs a rigid geometry having an O–H bond distance of 0.9572 Å, an H–O–H bond angle of 104.52°, and a massless, off-atom M site located 0.15 Å along the H–O–H bisector which carries the oxygen partial charge. Repulsion and dispersion interactions are modeled using a single Lennard–Jones (LJ) site located on the oxygen center having parameters $R_{\mathrm{min,O}}$ = 3.5459 Å and ε_{O} = 0.2862 kcal mol^{-1}.

Ions were treated as nonpolarizable particles with interaction parameters based on those by Lamoureux and Roux[65] and validated for use with TIP4P-FQ.[66−70] We acknowledge that the use of a mixed polarizable water model with nonpolarizable anion representation may appear unorthodox, but we consider that the combination of this *empirical* model is well-validated and reproduces many of the currently accepted experimental observables upon which the quality of such force fields are based. Furthermore, the use of an alternative force field model allows us to speak to the universality (or at least the broad commonality) of molecular and atomic features underlying observed behaviors such as surface stability and negative surface

dx.doi.org/10.1021/jp401243m | J. Phys. Chem. B XXXX, XXX, XXX−XXX

adsorption entropy. We summarize the parameters used in Table 1. The nonbond interactions were treated via the standard Lennard−Jones "12−6" potential

$$E_{LJ} = \sum_{ij} \varepsilon_{ij}\left(\frac{R_{\min,ij}^{12}}{r_{ij}^{12}} - 2\frac{R_{\min,ij}^{6}}{r_{ij}^{6}}\right) \quad (2)$$

Lennard−Jones interactions were gradually switched off at interparticle distance of 11 Å, with a gradual switching between 10 Å and 11 Å using the switching function:

$$S(r_{ij}) = \begin{cases} 1 & r_{ij} \le r_{on} \\ \dfrac{(r_{off}^2 - r_{ij}^2)^2(r_{off}^2 + 2r_{ij}^2 - 3r_{on}^2)}{(r_{off}^2 - r_{on}^2)^3} & r_{on} < r_{ij} \le r_{off} \\ 0 & r_{ij} > r_{off} \end{cases} \quad (3)$$

Charge degrees of freedom for the TIP4P-FQ water molecules were coupled to a thermostat at 1 K with mass 0.000069 kcal mol^{-1} ps^2 e^{-2} using the Nosé-Hoover method, and the charge degrees of freedom were propagated in an extended Lagrangian formalism; each water molecule was taken as a charge normalization unit (charge conserved with this unit), thus preventing any charge transfer between water molecules or between water and ion. We acknowledge recent developments of charge transfer models of water,[71,72] and anticipate that application of charge transfer models to the study of specific-ion effects will soon be realized and further elucidate underlying mechanisms and physics. Conditionally convergent long-range electrostatic interactions were treated using particle mesh Ewald (PME)[73] approach with a 30 × 30 × 128 point grid, sixth order interpolation, and κ = 0.33. Dynamics were propagated using a Verlet leapfrog integrator with a 0.5 fs time step. Total sampling time for each window was 15−20 ns; properties were calculated from all but the initial 0.5 ns, which was treated as equilibration.

Table 1. Parameters Used in This Study

	R_{min} (Å)	ε (kcal/mol)	q (e)
O[a]	3.5458	0.2862	−0.888
Cl^-	4.9198	0.07658	−1
I^-	5.5198	0.15910	−1

[a]Charge presented here was on the M-site of TIP4P-FQ water molecule in the gas phase.

For potential of mean force calculations, our reaction coordinate, ξ_0, is the Cartesian z-component of the separation between the water slab center of mass and ion center of mass. In all simulations used for computing potentials of mean force, ions were restrained to z-positions from 10 to 35 Å relative to the water slab center of mass using a harmonic potential $U_{restraint}(z; z_{relative,ref}) = (1/2)k_{restraint}(z - z_{relative,ref})^2$ with the force constant of 4 (kcal/mol)/Å^2; this encompasses a range approximately 15 Å below the Gibbs dividing surface (GDS) to approximately 10 Å above it at 300 K; though one could probe separations further into the bulk (toward the center of the system), this distance is sufficient to probe the differences of interest in this study, and also in keeping with previous studies to which we compare our results. In the case of 360 K, the highest temperature in this study, GDS increases by 2 Å. The actual position of GDS at corresponding temperature, which is determined by half of bulk water oxygen density, is plotted in Figure 1 (to be discussed in Results section). We note the

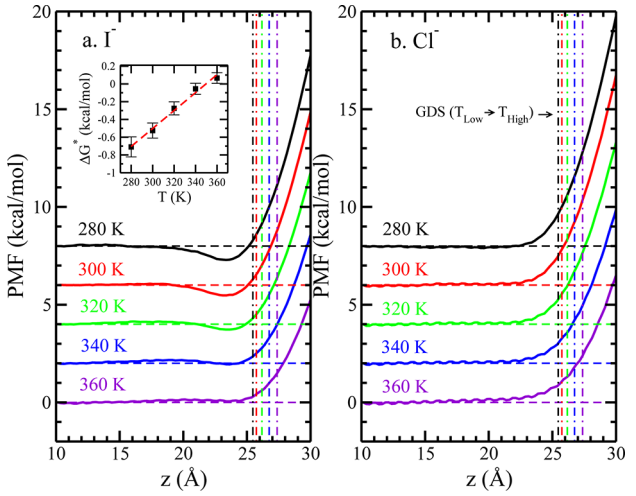

Figure 1. Potential of mean force for single (a) iodide and (b) chloride ions across the TIP4P-FQ LV-interface, relative to the value at z = 10.0 Å, which we consider sufficiently far away from the interface so as to represent bulk-like water region. Solid lines represent ions in TIP4P-FQ, a vertical offset of 2 kcal/mol is used to distinguish different temperature, each with a dashed horizontal line denoting zero. The inset shows the PMF minimum as the function of temperature for I^-. The dashed line indicates the linear fitting result, with slope = 0.01 and intercept = −3.53.

recent connection of the potential of mean force to thermodynamic free energies:[74]

$$\frac{dG(\xi_0)}{d\xi_0} = \left\langle \left(\frac{\partial U_{interaction}(r^N)}{\partial q_\xi}\right)_{\{q_{m\neq\xi}\}^{N-1}} \right\rangle_{\xi_0} - \left\langle \frac{1}{\beta}\left(\frac{\partial \ln|J|}{\partial \xi}\right)_{\{q_{m\neq\xi}\}^{N-1}} \right\rangle_{\xi_0} - \frac{1}{\beta}\left\langle \sum_{m\neq\xi}^{N-1}\left[\delta(q_m - l_{U_m})\frac{dl_{U_m}(q_m)}{dq_\xi}\delta(q_m - l_{L_m})\frac{dl_{L_m}(q_m)}{dq_\xi}\right]\right\rangle_{\xi_0} \quad (4)$$

where the interaction potential is taken to be a function of some set, of the size of the number of system degrees of freedom, of generalized coordinates, q_ξ. The reaction coordinate of interest in this case corresponds to $q_\xi = \xi_0$. The first term is the negative of the mean force whose integral over the domain of the reaction coordinate yields the potential of mean force. The second term arises from the volume scaling upon transforming from Cartesian to some generalized curvilinear space (represented in general by the set of generalized coordinates). The last term arises from interchange of the order of the differential and integral operators according to Leibniz rule. In the present study, as we retain the Cartesian z-component of the separation between centers of mass (the force is projected along this reaction coordinate), and the domain of the reaction coordinate is decoupled from those of

dx.doi.org/10.1021/jp401243m | J. Phys. Chem. B XXXX, XXX, XXX−XXX

the remaining coordinates (the derivatives in the Leibniz term are zero), the Jacobian and Leibniz terms vanish. Thus, we discuss the PMF in terms of the free energy or reversible work for the remainder of the paper.

III. RESULTS AND DISCUSSION

A. Potential of Mean Force and Solvation Structure. The potential of mean force ($\Delta G(z)$) was calculated for each ion as a function of its z-position using WHAM[55] and is referenced to zero at z = 10 Å; results of I^- and Cl^- at different temperatures are shown in Figure 1 a and b, respectively. For clarity, a vertical offset of 2 kcal/mol is added to distinguish the PMF at different temperatures. While Cl^- shows no pronounced minimum independent of temperature, I^- shows minima below the GDS at all temperatures except 360 K. We define ΔG^* as the PMF at the minimum and plot it as a function of temperature, as shown in the inset of Figure 1a along with the uncertainty and the linear fitting result ($\Delta G^* = \Delta H^* - T\Delta S^*$). We observe a positive slope for ΔG^* versus T indicating $\Delta S^* < 0$. The uncertainties in potentials of mean force are determined using the approach of Zhu and Hummer:[75]

$$\mathrm{var}[G(\xi_N)] \approx \sum_{i=1}^{N} \mathrm{var}[K\Delta\xi\bar{z}_i] \tag{5}$$

where $\bar{z}_i$ is the mean position of z in the ith window, which can be obtained from block averages.[76] The corresponding standard deviation $\sigma[G(\xi_N)]$ is then the square root of $\mathrm{var}[G(\xi_N)]$. In our case, $G(z = 10\ \text{Å}) = 0$, and therefore, the window z = 35 Å is expected to have the largest uncertainty. The largest uncertainties for the systems are approximately 0.13 kcal/mol (shown in the Supporting Information).

At 300 K, I^- shows a minimum of 0.5 kcal/mol, which is similar to the result for iodide at the L-V interface using nonpolarizable ions in SPC/E water by Horinek et al.[25,53] This also corresponds with the DFT-D value determined by Baer and Mundy,[43] though we do not discount that ours is a fortuitous result to some degree. In our simulation, we do not include explicitly the polarization of the I^-, but we have taken care to faithfully capture the relative hydration free energetics of the individual ions to as great an extent as possible. Though not possible currently, it would be interesting to connect the hydration free energetics of ions using DFT-D methods in order to further assess and characterize such agreements between classical models and electron-density based models. Caleman et al.[50] observed a significantly deeper free energy minimum (≈1.4 kcal/mol) for similar calculations but using water droplets and a polarizable force field based on classical Drude oscillators for water[77] and ions;[65] the force fields used in that study were parametrized to optimally recapitulate experimental hydration free energies of ions in bulk water and ion−water binding energies and geometries of gas-phase water−ion dimer complexes.[65] Later studies have concluded that the greater stability suggested by such classical models may arise from a representation of ion and water polarization response that is larger than the actual physical value. What appears in general, however, is that the location of the PMF minimum occurs prior to the GDS (defined in terms of the water density in most studies).

An intriguing property that seems to be universal among the single anion PMFs estimated using various parametrized classical models (nonpolarizable and polarizable, including the present study) is the emergence of a perceptible barrier before the surface-stable anions reach the Gibbs dividing surface;[16,25,50,69] this barrier is even observed for polarizable ions at the water−CCl_4 interface.[18] Despite its prevalence, this feature has not been addressed to any significant extent. We conjecture at the present time that several factors (not necessarily confined to regions local to the ion and its vicinal hydration shell) give rise to a real physical barrier. The observation of this barrier even in the DFT-D study and the dielectric continuum theory-based predictions[43] provides further compelling motive to pursue this feature found in PMF's based on numerous, widely differing interaction models. This is ongoing work and beyond the scope of the present study. Finally, unlike the study by Horinek,[25,53] however, we do not observe a minimum as the I^- moves across the L-V interface at T = 360 K. This suggests that underlying temperature-dependent properties of water−water and water−ion interactions are not equivalent; though not pursued presently, a comparison of the phase-equilibrium properties of the water−water interaction models used in the two studies would provide further insight as to the origins of this difference.

We next decompose our PMF into total enthalpic and total entropic components, acknowledging that this analysis is not a definitive exploration of the inherent driving forces for surface adsorption as observed via molecular simulations using classical force fields. It does allow some connection to previous studies using droplet based simulations[50] so as to allow one to draw conclusions about general behaviors and trends related to observed behaviors in anion surface propensities. In our system the pressure-volume work is negligible and so we will estimate enthalpic contributions with internal energy components. Furthermore, since we are interested in differences relative to specific positions in our simulation system, we will consider kinetic contributions to be equivalent at the end points, thus leaving us with interaction energy components as the determinants of the enthalpy changes. As in previous studies, we consider the enthalpy change $\Delta H(z)$ as the difference of average interaction potential energy[50,78,79] when the anion resides at position z and in bulk (z = 10 Å), $\Delta H(z) = H(z_{\text{ion}}) - H(z_{\text{bulk}})$. The entropy change profile, $\Delta S(z)$, can therefore be estimated by subtracting enthalpy from free energy, $-T\Delta S(z) = \Delta G(z) - \Delta H(z)$. Figure 2 shows the enthalpic component $\Delta H(z)$ and entropic component $-T\Delta S(z)$ of the free energy for I^- and Cl^-. For clarity, we added 5 and −5 kcal/mol vertical offsets for $\Delta H(z)$ and $-T\Delta S(z)$, respectively. At 300 K, relative to when the ion is located in a bulk-like z-position, the total system enthalpy for states where I^- is surface-adsorbed is lower, while the enthalpy for Cl^- (not surface-enhanced in our study) effectively does not change at the GDS. Caleman et al.[50] observed a similar, though slightly deeper, minimum for I^-. Furthermore, the present relative enthalpies are not overly temperature sensitive. Entropy contributions are positive, suggesting inherent negative adsorption entropy as evidenced by the fitting slope of 0.01 kcal/mol/K obtained from a linear fit of the temperature versus PMF well-depth data. Negative surface adsorption entropy has been concluded from experiment[49] and from theory and simulations[25,49]

We further decompose $\Delta H(z)$ into water−water (w-w) and ion−water (i-w) contributions,[50] which are represented by the averaged potential energy at each window. These potential energies are plotted relative to the window where the anion is restrained at z = 10 Å, such that

dx.doi.org/10.1021/jp401243m | J. Phys. Chem. B XXXX, XXX, XXX−XXX

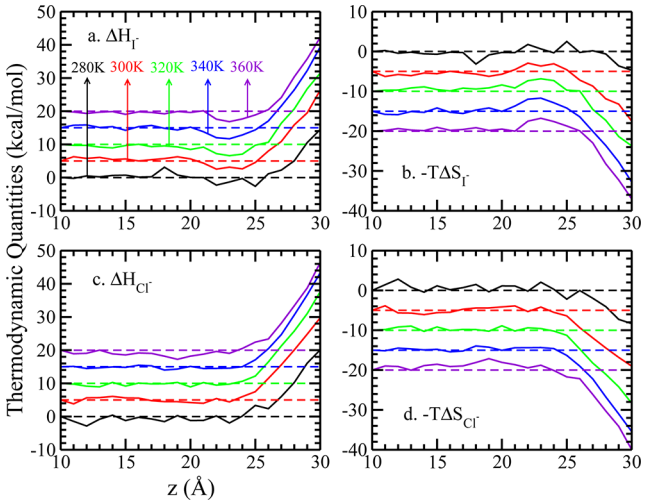

Figure 2. Decomposition of (a, c) enthalpic and (b, d) entropic contributions to the potential of mean force of single iodide and chloride ion crossing the TIP4P-FQ LV-interface, relative to the value at z = 10.0 Å. A vertical offset of 5 kcal/mol is used in panels (a) and (c), while in panels (b) and (d) the vertical offset is −5 kcal/mol, for clarity.

$$\Delta H(z) = \Delta H_{w-w}(z) + \Delta H_{i-w}(z) \quad (6)$$

The results of $\Delta H_{w-w}(z)$ and $\Delta H_{i-w}(z)$ of I^- and Cl^- are shown in Figure 3. In the case of I^-, $\Delta H_{w-w}(z)$ shows a

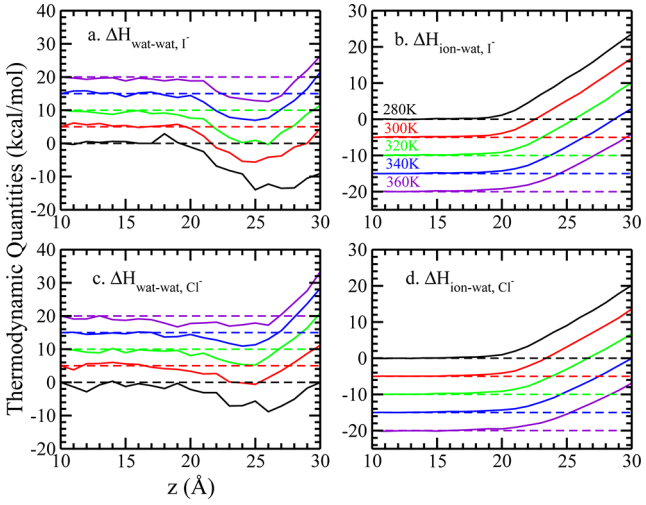

Figure 3. Decomposition of enthalpic contributions into (a, c) water−water and (b, d) ion−water interactions of single iodide and chloride ion crossing the TIP4P-FQ LV-interface, relative to the value at z = 10.0 Å. A vertical offset of 5 kcal/mol is used in panels (a) and (c), while in panels (b) and (d) the vertical offset is −5 kcal/mol, for clarity.

significant minimum at z = 25 Å, which is closer to the GDS than the minimum of $\Delta G(z)$ and $\Delta H(z)$ at z = 23 Å; at this z-position, the ion−water interaction is positive, thus restricting the minimum of the total enthalpy to below the GDS. The combination of water−water and water−ion enthalpies (interaction energies) effectively cancel one another, leading to the flat profile of the Cl^- total enthalpy, though Figure 3 indicates that the water−water interaction in the Cl^- case does reach a minimum at the GDS location. We define $\Delta H^{\dagger}_{w-w}$ as the minimum of ΔH_{w-w}, $\Delta H^{\dagger}_{i-w} = \Delta H_{i-w}(GDS) - \Delta H_{i-w}(10\ Å)$, and $\Delta H^{\ddagger}_{i-w} = \Delta H_{i-w}(35\ Å) - \Delta H_{i-w}(10\ Å)$ and list these values in Table 2. Although no significant minimum for $\Delta G(z)$ and

Table 2. Decomposition of $\Delta H(z)$ into Water−Water and Ion−Water Components at Some Significant z-Positions[a]

system	$\Delta H^{\dagger}_{w-w}$	$\Delta H^{\dagger}_{i-w}$	$\Delta H^{\ddagger}_{i-w}$
I^-			
280 K	−13.97	11.35	37.17
300 K	−10.62	10.18	34.90
320 K	−10.31	8.83	32.50
340 K	−8.04	7.42	29.58
360 K	−7.38	7.84	27.11
Cl^-			
280 K	−8.85	11.22	31.92
300 K	−5.61	8.11	30.02
320 K	−4.78	6.97	27.53
340 K	−4.08	4.10	25.38
360 K	−3.06	3.20	23.16

[a]Refer to text for the detail definition. The units are in kcal/mol.

$\Delta H(z)$ has been found for Cl^-, we still observe a minimum for $\Delta H_{w-w}(z)$. These minima, while shallower compared with those in the I^- system, show the same temperature dependence. For both anions, $\Delta H_{i-w}(z)$ terms monotonically increase as the ion approaches the vapor phase independent of temperature. We finally break down the total enthalpy into electrostatic and dispersion contributions. We can write eq 6 as

$$\begin{aligned}\Delta H(z) &= \Delta H_{vdW}(z) + \Delta H_{elec}(z) \\ &= \Delta H_{vdW,w-w}(z) + \Delta H_{vdW,i-w}(z) \\ &\quad + \Delta H_{elec,w-w}(z) + \Delta H_{elec,i-w}(z)\end{aligned} \quad (7)$$

We plot the $\Delta H_{elec,w-w}(z)$ and $\Delta H_{elec,i-w}(z)$ terms in Figure 4. Again, we set z = 10 Å as the reference for both cases. Comparison of Figures 4 and 3 shows that electrostatics dominate both water−water and ion−water interactions.

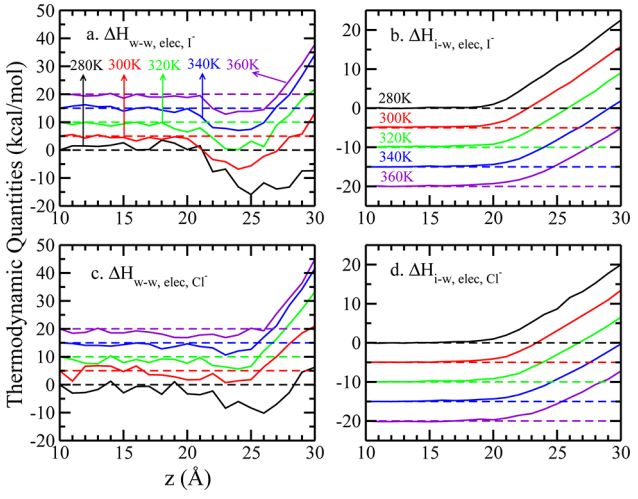

Figure 4. Decomposition of the electrostatic component of enthalpic contributions. Panels (a, c) show the electrostatic contribution to the water−water interactions and (b, d) refer to the ion−water interactions. Values are all relative to the value at z = 10.0 Å. A vertical offset of 5 kcal/mol is used in panels (a) and (c), while in panels (b) and (d) the vertical offset is −5 kcal/mol, for clarity.

dx.doi.org/10.1021/jp401243m | J. Phys. Chem. B XXXX, XXX, XXX−XXX

We consider the change in hydration of ions through the LV-interface by calculating the number of coordination water molecules as a function of z-position ($\langle N_{coor}\rangle$, Figure 5 c and d); this addresses the difference of $\Delta H_{i-w}(z)$. We define the first solvation shell cutoff distance as the first minimum of the anion-oxygen radial distribution function, as shown in Figure 5a and b. Moving through the GDS into the vapor, the coordination number decreases. All ions remain partially hydrated in the vapor; both anions maintain about four coordinating water molecules. Completely desolvated ions are not observed in our simulations. This is in agreement with calculations for transferring hydrated ion clusters from bulk water to 1,2-dichloroethane,[80] and simulations of ions across water/air interface.[16] As the larger ion, I^- inherently has more water molecules in the first solvation shell, and thus experiences greater changes in its coordination environment upon transfer into the vapor phase. Since the ion-coordinated water interaction is negative, this reduction of $\langle N_{coor}\rangle$ as the ion moves past the GDS result in the increase of $\Delta H_{i-w}(z)$. The larger change in $\langle N_{coor}\rangle$ for I^- necessarily leads to larger $\Delta H_{i-w}(z)$ for I^- than Cl^- at the same temperature. As the temperature increases, both ions show less reduction of $\langle N_{coor}\rangle$, and therefore leads to less ΔH_{i-w}.

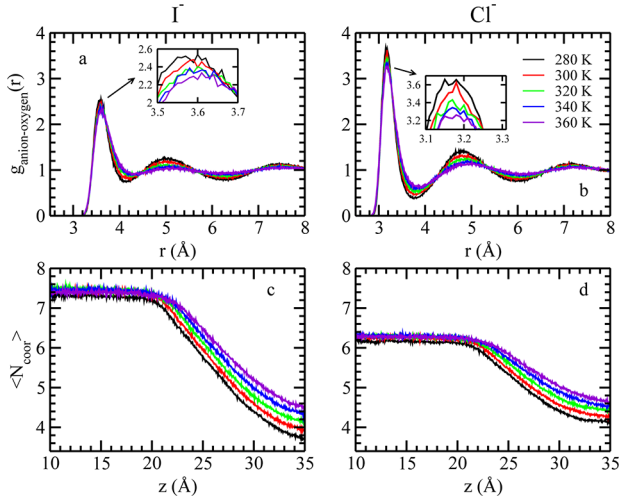

Figure 5. Anion-oxygen radial distribution function (RDF) for (a) I^- and (b) Cl^- at different temperatures. Average number of coordinated water for (c) I^- and (d) Cl^- at different temperatures.

Thus far, our analysis of the global enthalpy change indicates that the balance of water−water and water−ion interactions through the interface result in the enthalpy minimum before the GDS in the I^- system. Since the water−water interaction component of the enthalpy yields the largest favorable contribution (Figure 3), we now adopt the analysis of Otten et al.[49] to consider the origin of this contribution, and its sign, based on consideration of the average interaction energy of a water molecule with other water molecules in the system; we consider this average interaction energy for the regions where the water molecule is in a bulk-like region, at the liquid−vapor interfacial region, and in the hydration shell of the anion. The total water−water energy is $\langle U_{w-w}(z)\rangle = \bar{\varepsilon}_{coor}N_{coor}(z) + \bar{\varepsilon}_{L-V}N_{L-V}(z) + \bar{\varepsilon}_{bulk}N_{bulk}(z)$, where $\bar{\varepsilon}$ represents the average interaction energy of a water molecule with all the other water molecules in the corresponding environment. Here, N_{coor} indicates the number of water molecules within the first solvation shell of the ion, N_{L-V} refers to water molecules near the GDS but not within the first solvation shell of the ion, and finally, N_{bulk} refers to the water molecules that are in the bulk liquid (but not within the coordination criteria or near the L-V interface). $\Delta H_{w-w}(z)$ is therefore

$$\Delta H_{w-w}(z) = \bar{\varepsilon}_{coor}\Delta N_{coor}(z) + \bar{\varepsilon}_{L-V}\Delta N_{L-V}(z) + \bar{\varepsilon}_{bulk}\Delta N_{bulk}(z) \quad (8)$$

where ΔN is the difference in the number of water molecules in the region indicated by the subscript to ΔN; here, we adopt the definition of $\Delta N = N(z) - N(z = 10\ \text{Å})$. Since the total number of water molecules is fixed, we have $\Delta N_{bulk} = -(\Delta N_{coor}+\Delta N_{L-V})$, and therefore eq 8 can be written as

$$\Delta H_{w-w}(z) = (\bar{\varepsilon}_{coor} - \bar{\varepsilon}_{bulk})\Delta N_{coor}(z) + (\bar{\varepsilon}_{L-V} - \bar{\varepsilon}_{bulk})\Delta N_{L-V}(z) \quad (9)$$

In Figure 6, we present the density profile of water oxygen atoms along the z-dimension when an ion is restrained in bulk (z = 10 Å) or at the GDS. From Figure 6 c,d and previous discussion, we have ΔN_{L-V} and $\Delta N_{coor} < 0$. Since $\bar{\varepsilon}_{coor}$ and $\bar{\varepsilon}_{L-V}$ are both more positive than $\bar{\varepsilon}_{bulk}$, we obtain that $\Delta H_{w-w}(GDS)$ is negative. This recapitulates the results of Otten et al.[49]

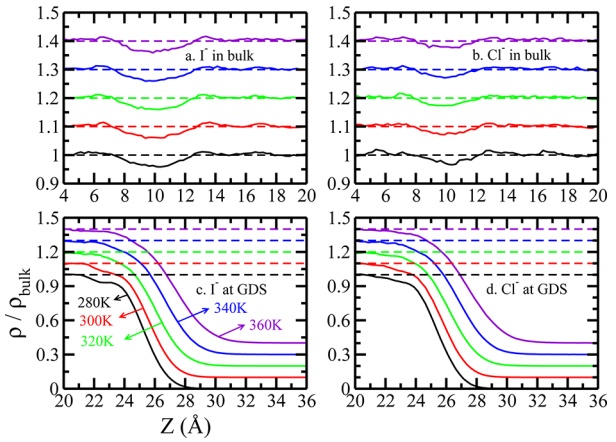

Figure 6. Density profile of water oxygen along z-dimension, when (a) I^- and (b) Cl^- are in the bulk (z_{ion} = 10 Å). The lower panels show the density profile along when (c) I^- and (d) Cl^- are at GDS, which is pushed toward the vapor phase as the temperature increases. An offset of 0.1 is added for clarity.

When the ion is in bulk, the number of bulk water molecules is reduced (the ions carve out a void that excludes water molecules); as the ion moves to GDS, water fills in the void, leading to $\Delta N_{bulk} > 0$, which is a reflection of the change of ΔN_{coor} and ΔN_{L-V}. From Figure 6a and b, we observe larger voids for I^- compared to those for Cl^-, which explains why ΔH_{w-w}(GDS) is more stabilizing for the larger anion. The size of these voids is not sensitive to the temperature. However, due to lower water−water interaction at high temperature (as evidenced by the shift of GDS to larger value as the water cohesive energy is reduced at elevated temperatures), we expect a less stabilizing $\Delta H_{w-w}(GDS)$ at elevated temperatures, shown in Figure 3a and c.

B. Surface Height Fluctuation and Entropy. From Figure 2 and earlier studies, it is acknowledged that surface-adsorption of anions at the aqueous liquid−vapor interface is an entropically disfavored process.[49,53,54] Intriguing ideas about

dx.doi.org/10.1021/jp401243m | J. Phys. Chem. B XXXX, XXX, XXX−XXX

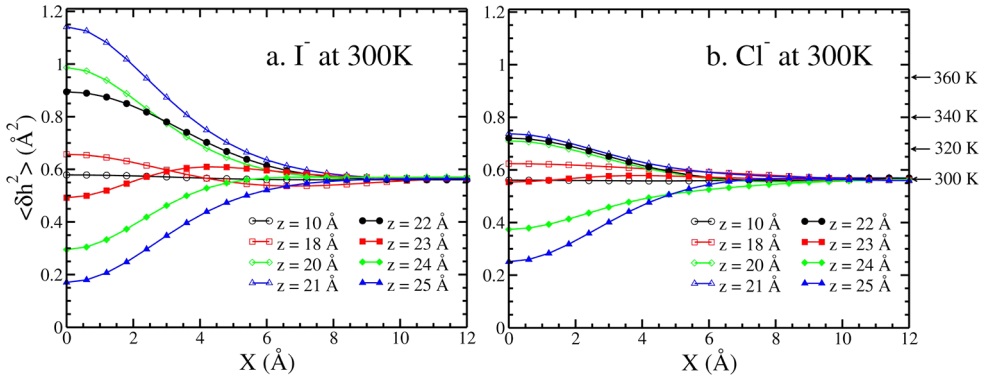

Figure 7. Surface height fluctuations, as functions of lateral displacement X (when the other lateral displacement Y is zero), for (a) I^- and (b) Cl^- reside in different restrained window at 300 K. The arrows in the right axis indicate the inherent pure water fluctuations from 300 to 360 K.

the origin of this negative entropy have emerged in recent literature[49,54] relating to the suppression of the fluctuations of the interface. Using the idea of coarse-graining atomically resolved interfaces, Otten et al.[49] showed using molecular simulations the reduction of interface fluctuations and the concomitant negative $\Delta S_{adsorption}$ calculated from the covariance matrix of interface fluctuations. We thus explore the nature of interfacial fluctuations in the two anion systems. In particular, we are interested in observing how fluctuations of the interface vary as the two ions approach the GDS and move through it. Since we have systems with unequivocal differences in surface-stability (i.e., one anion is stable at 300 K and the other shows no surface state), we hope to extract a strong correlation between surface stability and the perturbations induced by the two anions. We consider the fluctuations at 300 K first to set a baseline, and then consider the temperature dependence of induced interface fluctuations.

For an instantaneous surface snapshot, the local density profile can be defined as[81]

$$\left\langle \rho(\vec{r}_{xy}, z) \right\rangle \equiv \frac{1}{A_\xi} \int \mathrm{d}^2\vec{r}'_{xy}\, \rho(\vec{r}_{xy} - \vec{r}'_{xy}, z) = \rho[z - h(\vec{r}_{xy})] \tag{10}$$

which describes the short-distance average of the density over an area $A_\xi \sim \xi^2$ at position $\vec{r}_{xy}$. ξ is an inherent correlation length. Here we define $\delta h(\vec{r}_{xy}) = h(\vec{r}_{xy}) - z$ as a surface height function. With this definition, $\langle \delta h(\vec{r}_{xy}) \rangle = 0$.

From individual snapshots/configurations, we construct the coarse-grained instantaneous surface defined by Willard and Chandler.[82] Gaussian mass distributions are assigned to each water oxygen atom according to

$$\Phi(\mathbf{r};\, \xi) = (2\pi\xi^2)^{-d/2} \exp(-r^2/2\xi^2) \tag{11}$$

where r is the magnitude of $\mathbf{r}$, ξ is taken as 3.0 Å, and d is the dimensionality (3 in this case). At space-time point ($\mathbf{r}$, t), we have the coarse-grained density as

$$\bar{\rho}(\mathbf{r},\, t) = \sum_j \Phi(|\mathbf{r} - \mathbf{r}_j(t)|;\, \xi) \tag{12}$$

The interface is determined as the $(d - 1)$-dimensional manifold with constant value c. In practice, we set up a series of spatial grid points (x,y,z) and compute the corresponding coarse-grained densities $\rho(x,y,z)$ by eq 12. We use a grid spacing in the x and y dimensions of 0.6 Å; for the z dimension the grid resolution is 0.1 Å. The surface is then obtained as the manifold by setting $\rho(x,y,z) = \rho_{bulk}/2$. With sufficient sampling, we can average these instantaneous surfaces $(h_t(x,y)$, at time $t)$ and get the mean surface $\langle h(x,y) \rangle$; furthermore, $\langle \delta h(x,y) \rangle = 0$. Subtracting the mean values from the $h_t(x,y)$, we obtain $\delta h_t(x,y)$ and the height fluctuations $\delta h_t^2(x,\, y)$. Using this framework to characterize interface fluctuations, we can probe the magnitudes of interface fluctuations when the ions reside at various positions along the reaction coordinate. We first consider how the two anions affect the interface as they approach the interface at 300 K; then we discuss how these influences vary with temperature.

Figures 10−12 in the Supporting Information show representative instantaneous surfaces, mean surfaces, and fluctuations derived based on the above approach. In Figure 7 (main text), we show for 300 K the absolute magnitude of the mean interface fluctuation when I^- and Cl^- reside at various z-positions. The X-axis is the distance along the X-dimension for a coordinate system originating at the center of the anion. At 300 K, the inherent interface fluctuations for this water model are 0.56 (far way from the ion, X = 12 Å). We use this value as a proxy to represent the pure water interface fluctuations, but we have confirmed independently that these match the system of a pure water liquid−vapor interface in the absence of ions. Interestingly, the pure water interfacial fluctuations we obtain for the TIP4P-FQ water model are quite close to those reported by Otten et al. Approaching the interface, the mean fluctuations increase, with I^- inducing significantly larger perturbation than Cl^-. Since thermal fluctuations give rise to an inherent (absence of ions) level of interfacial fluctuations, we normalize the absolute mean surface fluctuations ($\langle \delta h^2(x,y) \rangle$) with the value for pure water at the corresponding temperature ($\langle \delta h_{pure}^2 \rangle$). Thus, when the ratio between $\langle \delta h^2(x,y) \rangle$ and $\langle \delta h_{pure}^2 \rangle$ (which is defined as $\langle \delta h_L^2 \rangle$) equals 1, the effect of ion is zero. When $\langle \delta h_L^2 \rangle > 1$, the surface height fluctuation is enhanced relative to pure water with the presence of ion; when $\langle \delta h_L^2 \rangle < 1$, the surface height fluctuation is suppressed.

Figure 8 shows the normalized, mean-square amplitude of surface height fluctuations as a function of lateral distance X from the ion. Generally, when the ion is 4 Å below the GDS, the fluctuations are maximum just above/beneath the ion (X = 0 Å). As the ion moves closer to the GDS, the fluctuation is reduced; when the ion resides at the GDS (z = 25 Å), the fluctuations are suppressed relative to pure water. The enhancement of fluctuations is related to the solvent spatial perturbations by the anion. The radial distribution functions of Figure 6a and b demonstrate that the solvent around the ion is

dx.doi.org/10.1021/jp401243m | J. Phys. Chem. B XXXX, XXX, XXX−XXX

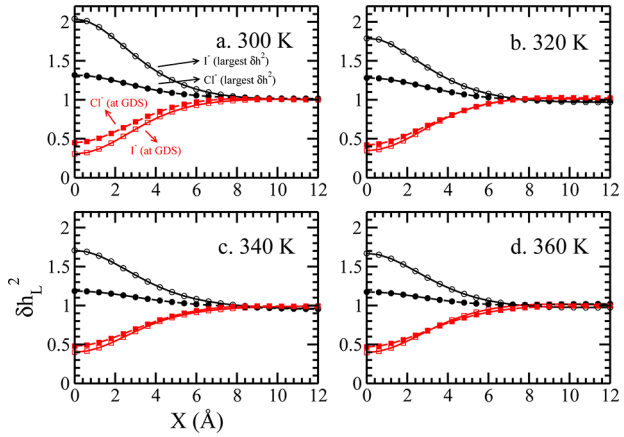

Figure 8. Normalized surface height fluctuations, as functions of lateral displacement X (when the other lateral displacement Y is zero), for ions at (a) 300 K, (b) 320 K, (c) 340 K, and (d) 360 K. Only the windows with largest δh_L^2 and the window of GDS are shown here. For other windows, please refer to the Supporting Information.

perturbed out to at least 8 Å away from the ion, suggesting that the presence of the ion generates interfacial perturbations before even reaching the vicinity of the GDS. As the ions approach the L-V interface, solvation shell water interferes with the interfacial water; inherent surface fluctuations are amplified, and reach a maximize when the edge of the first hydration shell (refer to the first minimum of RDF in Figure 5, which is approximately 3.8 and 4.2 Å for Cl^- and I^- at 300 K, respectively) coincides with the GDS.

From Figure 8a, a lower enhancement of surface fluctuations is associated with Cl^- relative to I^-. We posit that this is related to the coupling of the local anion solvation shell properties to the more distal solvent. The first solvation shell of Cl^- is more rigid and less "malleable" than that of I^-. Indications for this are as follow. The radial distribution functions, Figure 5, show a more dramatic ordering of water in the first solvation shell of Cl^-; this is widely known based on previous simulation studies.[65] We have also confirmed (data not shown) that the lifetime of water molecules in the first solvation shell of Cl^- are longer than of those in I^-'s first shell; furthermore, the velocity decorrelation times of first solvation shell water around Cl^- are shorter than those for I^-, and velocity correlation functions of first solvation shell water molecules around Cl^- retain an oscillatory "hump" indicative of water "rattling in a cage" formed from its closely packed nearest neighbors. Further evidence of the distinct environments of the first hydration shells of I^- and Cl^- are shown in Figures 17 and 18 of the Supporting Information. The average molecular dipole moment of water in the first solvation shell of Cl^- is significantly more enhanced than that in the first shell of I^-; the tetrahedrality of water in the first shells also demonstrates this difference. In total, these indications suggest that coordinated water molecules surrounding Cl^- are more "ordered" (vis-a-vis, rigid) compared to those around I^-. This being the case, the local water molecules around Cl^- (first to second solvation shell) are not as deformable; thus, when Cl^- nears the interface, the shielding effect of first (and somewhat second) solvation shell water molecules prevents significant added fluctuations of the interface. In fact, since Cl^- shows no surface state, we interpret the slight enhancement of interface fluctuations in the Cl^- case to be insignificant. Since the surface stability observed for these two anions is binary (I^- = on, Cl^- = off), we consider that there is a possible threshold of induced fluctuations separating surface-stable anions. Interestingly, Otten et al. demonstrate an ostensibly similar behavior in Figure S2 of the Supporting Information of that work.

We comment on the slight differences in the extent to which interfacial flucuations are suppressed once the ions reach the GDS and move through the interface. The slightly weaker suppression by Cl^-, we suggest, is due to the less anisotropic solvation structure (refer to Supporting Information or ref[69,83]) of Cl^- at the GDS. For the case of I^-, water molecules are rarely found above the ion, therefore the coarse-grained surfaces are mostly beneath I^-; however, for Cl^- there are more instantaneous coarse-grained surfaces observed above the anion resulting in slightly higher fluctuations than the case of when I^- resides at the GDS.

In summary, though Cl^- induces a much more modest perturbation, we consider this a noneffect. Considering that the I^- is surface-stable and the Cl^- not, this seems to suggest that there may exist a force field dependent critical level of perturbation of the interface that distinguishes between surface-stable and nonsurface stable species. This is conjecture at this time, but we continue to explore this idea with ongoing work. Nevertheless, the notion that Cl^- has no effect on interfacial fluctuations, correlating with its lack of surface stability, has implications when considering the temperature dependence of induced interfacial fluctuations, to which we now turn.

As temperature increases, the maximum of $\langle \delta h_L^2 \rangle$ for I^- drops from 2 to 1.65; on the other hand, the maximum of $\langle \delta h_L^2 \rangle$ for Cl^- is rather insensitive to temperature change, remaining approximately 1.3. Since the fluctuations of surface height can be decomposed into the ion-induced and water-inherent contributions, this indicates the fact that the proportion of ion-induced fluctuations is weakened as the temperature increases. We rationalize this by considering the mechanism through which I^- effects its perturbation. Since the perturbation of solvent structure amplifies the inherent interface fluctuations at lower temperatures, the increase of inherent fluctuations at higher temperatures reduces the impact of any solvent structural perturbation induced by the ion. Again, the reduction in the magnitude of interface fluctuation induced by I^- correlates with reduction in surface stability. Interestingly, we find that the absolute change in fluctuation magnitude from 12 Å to 0 Å is about 0.4, independent of temperature (for I^-) (though the value we ascribe to the end points would change based on characteristics of the grid used to estimate the instantaneous interfaces, the argument would sill hold).

Finally, we provide some estimates of surface entropy related to enhanced interface fluctuations in the presence of anions. We use concepts from multivariate statistics as discussed by Otten et al to formulate entropy estimates. For a random variable x with continuous density $f(x)$, the entropy can be written as[84]

$$S(f) = -\int_{-\infty}^{\infty}\int_{-\infty}^{\infty}\cdots\int_{-\infty}^{\infty} \ln[f(x)]\, f(x)\, dx \qquad (13)$$

where $x = (x_1, x_2, \cdots, x_N)'$. The density function of the multivariate normal distribution is given by

$$f(x) = \frac{1}{|2\pi\Sigma|^{1/2}} \exp\left\{-\frac{1}{2}(x-\mu)'\Sigma^{-1}(x-\mu)\right\} \qquad (14)$$

dx.doi.org/10.1021/jp401243m | J. Phys. Chem. B XXXX, XXX, XXX−XXX

Σ is the covariance matrix, $\Sigma_{ij} = \mathrm{cov}(x_i,x_j) = E[(x_i-\mu_i)(x_j-\mu_j)]$, where $\mu_i = E(x_i)$ is the expected value of the ith entry of x. We can therefore rewrite the entropy as

$$\begin{aligned} S &= \frac{1}{2}\{N + N\ln(2\pi) + \ln|\Sigma|\} \\ &= \frac{1}{2}\{\ln e^N + \ln(2\pi)^N + \ln|\Sigma|\} \\ &= \frac{1}{2}\ln\{(2\pi e)^N|\Sigma|\} \\ &= \frac{N}{2}\ln(2\pi e) + \frac{1}{2}\ln|\Sigma| \end{aligned} \tag{15}$$

where $|\Sigma|$ is the determinant of covariance matrix Σ. The surface entropy can therefore be estimated with surface height function $\delta h = h - \langle h\rangle$ since δh is normal distributed for each ion restrained-window (shown in the Supporting Information). The covariance matrix (χ) is then defined as $\chi_{ij} = \delta h_i \delta h_j$. The $(N/2)\ln(2\pi e)$ term is a constant for different windows with the same resolution of grid points (in other words, same N). Consequently, we get the entropy described by the fineness of the resolution of grid points:

$$S = \text{constant} + \frac{k_B}{2}\ln|\chi| \tag{16}$$

where k_B is the Boltzmann constant. We obtain ΔS as $\Delta S(z) = S(z) - S(z = 10\ \text{Å})$. For every 50 ps, we compute $\langle\chi\rangle$ and corresponding entropy. Eventually, we use these to get the estimation of $\langle S(z)\rangle$ (for convergence of entropy, please refer to the Supporting Information). The estimated $\langle\Delta S(z)\rangle$ for I^- and Cl^- between the window of highest fluctuations and bulk are listed in Table 3. As expected, the entropy at the position of highest interface fluctuations, z_1, relative to the bulk, $z = 10$ Å decreases with increasing temperature; values for Cl^- are smaller, also as anticipated based on differences in fluctuations. We reiterate that these are simply coarse estimates, with only qualitative descriptive value. These results recapitulate the idea put forth by Noah-Vanhoucke and Geissler that surface stable anions, in part, derive their thermodynamic stability through collective properties associated with the fluctuations of the interface and coupling of these with those fluctuations induced by the anions. Based on ion-induced interface fluctuations, the authors conclude that there is an entropic benefit for moving a volume-excluding ion from bulk to a position within the interface below the GDS; the free energy penalty for loss of electrostatic water−ion interactions becomes dominant after the passage of the anion through the GDS and into the vapor-like regions.[54]

Table 3. Estimated $\Delta S(z_1)$ and $\Delta S(z_{GDS})$ Obtained by the Covariance Matrix of Surface Height Functions[a]

system	$\Delta S(z_1)$	$\Delta S(z_{GDS})$
I^-		
300 K	31.80	−30.07
320 K	28.96	−28.98
340 K	23.35	−16.11
360 K	14.45	−14.13
Cl^-		
300 K	19.27	−11.61
320 K	15.21	−12.16
340 K	11.84	−9.59
360 K	14.13	−9.06

[a] z_1 indicates the window with largest fluctuations. The units are k_B.

IV. SUMMARY AND CONCLUSIONS

We have explored the enthalpic and entropic changes as two anions, I^- and Cl^-, cross the aqueous liquid−vapor interface under infinite dilution conditions; this variation is extracted from calculations of the potential of mean force associated with the reversible work involved with the translocation process. We find, in accord with numerous earlier experimental and simulation studies, that I^- has a modest surface stability of 0.5 kcal/mol, whereas Cl^- shows no such surface state. Coincidentally, our estimate of the surface stability (relative to bulk) for I^- is, most likely fortuitously, in agreement with the recent estimate by Baer et al. using DFT-D molecular dynamics (this is also in agreement with dielectric continuum theory approaches of Levin and co-workers). Decomposition of the potential of mean force is also in keeping with the results of Caleman et al. and Otten et al. We see that, at all temperatures, water−water interactions provide the sole favorable enthalpic contribution to the free energy while the water−ion interactions contribute a balancing destabilizing contribution until beyond the GDS, at which point the loss of water−ion interaction leads to the rapid increase in free energy. The temperature dependence study we present demonstrates that the surface adsorption process for anions is entropically disfavored, again in agreement with previous experiment and simulation studies. As suggested by Netz and Horinek,[53] the negative entropy of adsorption is independent of force field used, as further demonstrated in this study. Though the entropy is negative, we find that it is a small contribution to the entire process. We have explored one particular origin of this negative adsorption entropy, induced fluctuations of the aqueous liquid−vapor interface upon anion approach. We find that the surface-stable I^- induces significantly greater interfacial fluctuations (after accounting for inherent thermally-excited interface fluctuations) compared to Cl^-; at 300 K, the relative effect of I^- is a 2-fold increase of interface fluctuations in the immediate vicinity of the anion. We posit that the essence of the dramatic difference in the two anions' abilities to induce surface fluctuations lies in the properties of their respective local solvation shells, and the coupling of this local solvation shell with distal solvent. Specifically, Cl^-, being more charge-dense, carries a more rigid, ordered solvation shell (as evidenced by several solvation shell water properties discussed in the main text); this rigidity to some extent is conferred to the second solvation shell as well. I^- carries a much more malleable solvation shell. Approaching the interface, the long-range perturbations induced by both anions are more effectively damped by the local solvation shells of Cl^- compared to that of I^-; solvation structure perturbations are able to interact more easily with I^-'s solvation shell due to its malleability. In this picture, our interpretation is that the minimal perturbation of the interface by Cl^- is a noneffect; this interpretation is consistent with the unequivocally different surface-stabilities of the two anions (as computed using the models and attendant assumptions we have chosen for this work).

An implication of the mechanism through which I^- effects its perturbations of the interface is that increasing temperature of the solvent, thus enhancing inherent thermally excited fluctuations, should reduce the anions effect on surface

dx.doi.org/10.1021/jp401243m | J. Phys. Chem. B XXXX, XXX, XXX−XXX

fluctuations; likewise, since there is no effect from Cl^-, its effect should show no temperature dependence. Our results demonstrate that the relative contributions to changes in interface fluctuations from I^- decrease with temperature, while no perceptible change is present for Cl^-. This is again consistent with the decrease in surface-stability of I^- demonstrated by the disappearance of the free energy minimum before the GDS.

■ ASSOCIATED CONTENT

Supporting Information

Discussion of aspects of simulation protocol, details of the dipolement and tetrahedrality analysis of water, interaction energies of water with other water in the various regions (bulk, ion first solvation shell, and interface), and further details of the fluctuation analyses. This material is available free of charge via the Internet at http://pubs.acs.org.

■ AUTHOR INFORMATION

Corresponding Author

*E-mail: sapatel@udel.edu.

Notes

The authors declare no competing financial interest.

■ ACKNOWLEDGMENTS

The authors acknowledge partial support from the National Institutes of Health (COBRE:5P20RR017716-07) at the University of Delaware, Department of Chemistry and Biochemistry. This work is also partially supported by National Science Foundation CAREER AWARD (MCB-1149802) to S.P. We thank Professor Phillip Geissler and Patrick Shaffer for sharing code for analysis of interface fluctuations and resulting entropy. We acknowledge N. Patel for fruitful discussions and guidance throughout this work.

■ REFERENCES

(1) Perera, L.; Berkowitz, M. L. Many-Body Effects in Molecular Dynamics Simulations of Na^+ $(H_2O)_n$ and $Cl^-(H_2O)_n$ Clusters. *J. Chem. Phys.* **1991**, *95*, 1954−1963.

(2) Perera, L.; Berkowitz, M. L. Ion Solvation in Water Clusters. *Z. Phys. D* **1993**, *26*, 166−168.

(3) Vrbka, L.; Mucha, M.; Minofar, B.; Jungwirth, P.; Brown, E. C.; Tobias, D. J. Propensity of Soft Ions for the Air/Water Interface. *Curr. Opin. Colloid Interface Sci.* **2004**, *9*, 67−73.

(4) Jungwirth, P.; Tobias, D. J. Chloride Anion on Aqueous Clusters, at the Air-Water Interface, and in Liquid Water: Solvent Effects on Cl^- Polarizability. *J. Phys. Chem. A* **2002**, *106*, 379−383.

(5) D'Auria, R.; Tobias, D. J. Relation Between Surface Tension and Ion Absorption at the Air-Water Interface: A Molecular Dynamics Simulation Study. *J. Phys. Chem. A* **2009**, *113*, 7286−7293.

(6) Vazdar, M.; Pluhařová, E.; Mason, P. E.; Vácha, R.; Jungwirth, P. Ions at Hydrophobic Aqueous Interfaces: Molecular Dynamics with Effective Polarization. *J. Phys. Chem. Lett.* **2012**, *3*, 2087−2091.

(7) Knipping, E. M.; Lakin, M. J.; Foster, K. L.; Jungwirth, P.; Tobias, D. J.; Gerber, R. B.; Dabdub, D.; Finlayson-Pitts, B. J. Experiments and Simulations of Ion-Enhancement Interfacial Chemistry on Aqueous NaCl Aerosols. *Science* **2000**, *288*, 301−306.

(8) Brown, E. C.; Mucha, M.; Jungwirth, P.; Tobias, D. J. Structure and Vibrational Spectroscopy of Salt Water/Air Interfaces: Predictions from Molecular Dynamics Simulations. *J. Phys. Chem. B* **2005**, *109*, 7934−7940.

(9) Mucha, M.; Frigato, T.; Levering, L. M.; Allen, H. C.; Tobias, D. J.; Dang, L. X.; Jungwirth, P. Unified Molecular Picture of the Surfaces of Aqueous Acid, Base, and Salt Solutions. *J. Phys. Chem. B* **2005**, *109*, 7617−7623.

(10) Jungwirth, P.; Winter, B. Ions at Aqueous Interfaces: From Water Surface to Hydrated Proteins. *Annu. Rev. Phys. Chem.* **2008**, *59*, 343−366.

(11) Jungwirth, P.; Tobias, D. Surface Effects on Aqueous Ionic Solvation: A Molecular Dynamics Simulation Study of NaCl at the Air/Water Interface From Infinite Dilution to Saturation. *J. Phys. Chem. B* **2000**, *104*, 7702−7706.

(12) Heyda, J.; Vincent, J. C.; Tobias, D. J.; Dzubiella, J.; Jungwirth, P. Ion Specificity at the Peptide Bond: Molecular Dynamics Simulations of *N*-Methylacetamide in Aqueous Salt Solutions. *J. Phys. Chem. B* **2010**, *114*, 1213−1220.

(13) Jungwirth, P.; Tobias, D. J. Molecular Structure of Salt Solutions: A New View of the Interface with Implications for Heterogeneous Atmospheric Chemistry. *J. Phys. Chem. B* **2001**, *105*, 10468−10472.

(14) Jungwirth, P.; Tobias, D. J. Ions at the Air/Water Interface. *J. Phys. Chem. B* **2002**, *106*, 6361−6373.

(15) Jungwirth, P.; Tobias, D. J. Specific Ion Effects at the Air/Water Interface. *Chem. Rev.* **2006**, *106*, 1259−1281.

(16) Dang, L. X. Computational Study of Ion Binding to the Liquid Interface of Water. *J. Phys. Chem. B* **2002**, *106*, 10388−10394.

(17) Sun, X.; Wick, C. D.; Dang, L. X. Computational Study of Ion Distributions at the Air/Liquid Methanol Interface. *J. Phys. Chem. A* **2010**, *115*, 5767−5773.

(18) Wick, C. D.; Dang, L. X. Recent Advances in Understanding Transfer of Ions Across Aqueous Interfaces. *Chem. Phys. Lett.* **2008**, *458*, 1−5.

(19) Chang, T.; Dang, L. X. Recent Advances in Molecular Simulations of Ion Solvation at Liquid Interfaces. *Chem. Rev.* **2006**, *106*, 1305−1322.

(20) Wick, C. W.; Dang, L. X. Distribution, Structure, and Dynamics of Cesium and Iodide Ions at the H_2O-CCl_4 and H_2O-Vapor Interfaces. *J. Phys. Chem. B* **2006**, *110*, 6824−6831.

(21) Dang, L. X.; Chang, T. M. Molecular Mechanism of Ion Binding to the Liquid/Vapor Interface of Water. *J. Phys. Chem. B* **2002**, *106*, 235−238.

(22) Dang, L. X. A Mechanism for Ion Transport Across the Water/Dichloromethane Interface: A Molecular Dynamics Study Using Polarizable Potential Models. *J. Phys. Chem. B* **2001**, *105*, 804−809.

(23) dos Santos, A. P.; Diehl, A.; Levin, Y. Surface Tensions, Surface Potentials, and the Hofmeister Series of Electrolyte Solutions. *Langmuir* **2010**, *13*, 10778−10783.

(24) Levin, Y.; dos Santos, A. P.; Diehl, A. Ions at the Air-Water Interface: An End to a Hundred-Year-Old Mystery? *Phys. Rev. Lett.* **2009**, *103* (257802), 1−4.

(25) Horinek, D.; Herz, A.; Vrbka, L.; Sedlmeier, F.; Mamatkulov, S. I.; Netz, R. R. Specific Ion Adsorption at the Air/Water Interface: The Role of Hydrophobic Solvation. *Chem. Phys. Lett.* **2009**, *479*, 173−183.

(26) Enami, S.; Mishra, H.; Hoffmann, M. R.; Colussi, A. J. Hofmeister Effects in Micromolar Electrolyte Solutions. *J. Chem. Phys.* **2012**, *136* (154707), 1−5.

(27) Petersen, P. B.; Saykally, R. J. Confirmation of Enhanced Anion Concentration at the Liquid Water Surface. *Chem. Phys. Lett.* **2004**, *397*, 51−55.

(28) Petersen, P. B.; Saykally, R. J.; Mucha, M.; Jungwirth, P. Enhanced Concentration of Polarizable Anions at the Liquid Water Surface: SHG Spectroscopy and MD Simulations of Sodium Thiocyanide. *J. Phys. Chem. B* **2005**, *109*, 10915−10921.

(29) Petersen, P. B.; Saykally, R. J. Probing the Interfacial Structure of Aqueous Electrolytes with Femtosecond Second Harmonic Generation Spectroscopy. *J. Phys. Chem. B* **2006**, *110*, 14060−14073.

(30) Robertson, W. H.; Johnson, M. A. Molecular Aspects of Halide Ion Hydration: The Cluster Approach. *Annu. Rev. Phys. Chem.* **2003**, *54*, 173−213.

(31) Petersen, P. B.; Saykally, R. J. On the Nature of Ions at the Liquid Water Surface. *Annu. Rev. Phys. Chem.* **2006**, *57*, 333−364.

(32) Walker, D. S.; Richmond, G. L. Depth Profiling of Water Molecules at the Liquid-Liquid Interface Using a Combined Surface

Vibrational Spectroscopy and Molecular Dynamics Approach. *J. Am. Chem. Soc.* **2007**, *129*, 9446−9451.
(33) Walker, D. S.; Richmond, G. L. Understanding the Effects of Hydrogen Bonding at the Vapor-Water Interface: Vibrational Sum Frequency Spectroscopy of H_2O/HOD/D_2O Mixtures Studied Using Molecular Dynamics Simulations. *J. Phys. Chem. C* **2007**, *111*, 8321−8330.
(34) Richmond, G. L. Molecular Bonding and Interactions at Aqueous Surfaces as Probed by Vibrational Sum Frequency Spectroscopy. *Chem. Rev.* **2002**, *102*, 2693−2724.
(35) Liu, W.-T.; Zhang, L.; Shen, Y. R. Interfacial Structures of Methanol:Water Mixtures at a Hydrophobic Interface Probed by Sum-Frequency Vibrational Spectroscopy. *J. Chem. Phys.* **2006**, *125* (144711), 1−6.
(36) Chen, Z.; Ward, R.; Tian, Y.; Baldelli, S.; Opdahl, A.; Shen, Y. R.; Somorjai, G. A. Detection of Hydrophobic End Groups on Polymer Surfaces by Sum-Frequeny Generation Vibration Spectroscopy. *J. Am. Chem. Soc.* **2000**, *122*, 10615−10620.
(37) Levin, Y. Polarizable Ions at Interfaces. *Phys. Rev. Lett.* **2009**, *102*, 147803.
(38) Godec, A.; Merzel, F. Physical Origin Underlying the Entropy Loss Upon Hydrophobic Hydration. *J. Am. Chem. Soc.* **2012**, *134*, 17574−17581.
(39) Schelero, N.; von Klitzing, R. Correlation Between Specific Ion Adsorption at the Air/Water Interface and Long-Range Interactions in Colloidal Systems. *Soft Matter* **2011**, *7*, 2936−2942.
(40) Parsons, D. F.; Boström, M.; Nostro, P. L.; Ninham, B. W. Hofmeister Effects: Interplay of Hydration, Nonelectrostatic Potentials, and Ion Size. *Phys. Chem. Chem. Phys.* **2011**, *13*, 12352−12367.
(41) Herce, D. H.; Perera, L.; Darden, T. A.; Sagui, C. Surface Solvation for an Ion in a Water Cluster. *J. Chem. Phys.* **2004**, *122* (024513), 1−10.
(42) Arslanargin, A.; Beck, T. L. Free Energy Partitioning Analysis of the Driving Forces That Determine Ion Density Profiles Near the Water Liquid-Vapor Interface. *J. Chem. Phys.* **2012**, *136* (104503), 1−12.
(43) Baer, M. D.; Mundy, C. J. Toward an Understanding of the Specific Ion Effect Using Density Functional Theory. *J. Phys. Chem. Lett.* **2011**, *2*, 1088−1093.
(44) Baer, M. D.; Mundy, C. J. An ab initio Approach to Understanding the Specific Ion Effect. *Faraday Discuss* **2013**, *160*, 89−101.
(45) Baer, M. D.; Stern, A. C.; Levin, Y.; Tobias, D. J.; Mundy, C. J. Electrochemical Surface Potential Due to Classical Point Charge Models Drives Anion Adsorption to the Air-Water Interface. *J. Phys. Chem. Lett.* **2012**, *3*, 1565−1570.
(46) Kathmann, S. M.; Kuo, I. W.; Mundy, C. J. Electronic Effects on the Surface Potential at the Vapor-Liquid Interface of Water. *J. Am. Chem. Soc.* **2008**, *130*, 16556−16561.
(47) Kathmann, S. M.; Kuo, I. W.; Mundy, C. J.; Schenter, G. K. Understanding the Surface Potential of Water. *J. Phys. Chem. B* **2012**, *115*, 4360−4377.
(48) Rankin, B. M.; Hands, M. D.; Wilcox, D. S.; Fega, K. R.; Slipchenko, L. V.; Ben-Amotz, D. Interactions Between Halide Anions and a Molecular Hydrophobic Interface. *Faraday Discuss.* **2013**, *160*, 255−270.
(49) Otten, D. E.; Shaffer, P. R.; Geissler, P. L.; Saykally, R. J. Elucidating the Mechanism of Selective Ion Adsorption to the Liquid Water Surface. *Proc. Natl. Acad. Sci. U.S.A.* **2012**, *109*, 701−705.
(50) Caleman, C.; Hub, J. S.; van Maaren, P. J.; van der Spoel, D. Atomistic Simulation of Ion Solvation in Water Explains Surface Preference of Halides. *Proc. Natl. Acad. Sci. U.S.A.* **2011**, *108*, 6838−6842.
(51) Zhang, Y. J.; Furyk, S.; Bergbreiter, D. E.; Cremer, P. S. Specific Ion Effects on the Water Solubility of Macromolecules: PNIPAM and the Hofmeister Series. *J. Am. Chem. Soc.* **2005**, *127*, 14505−14510.
(52) Zhang, Y.; Cremer, P. S. Interactions Between Macromolecules and Ions: The Hofmeister Series. *Curr. Opin. Chem. Biol.* **2006**, *10*, 658−663.
(53) Netz, R. R.; Horinek, D. Progress in Modeling of Ion Effects at the Vapor/Water Interface. *Annu. Rev. Phys. Chem.* **2012**, *63*, 401−418.
(54) Noah-Vanhoucke, J.; Geissler, P. L. On the Fluctuations That Drive Small Ions Towards and Away From, Interfaces Between Polar Liquids and Their Vapors. *Proc. Natl. Acad. Sci. U.S.A.* **2009**, *106*, 15125−15130.
(55) Kumar, S.; Bouzida, D.; Swendsen, R. H.; Kollman, P. A.; Rosenberg, J. M. The Weighted Histogram Analysis Method for Free-Energy Calculations on Biomolecules. I. The Method. *J. Comput. Chem.* **1992**, *13*, 1011−1021.
(56) Brooks, B. R.; Books, C. L., III; MacKerell, A. D., Jr.; Nilsson, L.; Petrella, R. J.; Roux, B.; Won, Y.; Archontis, G.; Bartels, C.; Boresch, S.; et al. CHARMM: The Biomolecular Simulation Program. *J. Comput. Chem.* **2009**, *30*, 1545−1614.
(57) Nosé, S. A Molecular Dynamics Method for Simulations in the Canonical Ensemble. *Mol. Phys.* **1984**, *52*, 255−268.
(58) Rick, S. W.; Stuart, S. J.; Berne, B. J. Dynamical Fluctuating Charge Force Fields: Application to Liquid Water. *J. Chem. Phys.* **1994**, *101*, 6141−6156.
(59) Ryckaert, J. P.; Ciccotti, G.; Berendsen, H. J. C. Numerical Integration of the Cartesian Equations of Motion of a System with Constraints: Molecular Dynamics of *n*-Alkanes. *J. Comput. Phys.* **1977**, *23*, 327−341.
(60) Sanderson, R. T. *Chemical Bonds and Bond Energy*; Academic Press: New York, 1976.
(61) Rappe, A. K.; Goddard, W. A. Charge Equilibration for Molecular Dynamics Simulations. *J. Phys. Chem.* **1991**, *95*, 3358−3363.
(62) Rick, S. W.; Stuart, S. J.; Bader, J. S.; Berne, B. J. Fluctuating Charge Force Fields for Aqueous Solutions. *J. Mol. Liq.* **1995**, *65/66*, 31.
(63) Sanderson, R. T. An Interpretation of Bond Lengths and a Classification of Bonds. *Science* **1951**, *114*, 670−672.
(64) Warren, G. L.; Davis, J. E.; Patel, S. Origin and Control of Superlinear Polarizability Scaling in Chemical Potential Equilization Methods. *J. Chem. Phys.* **2008**, *128* (144110), 1−14.
(65) Lamoureux, G.; Roux, B. Absolute Hydration Free Energy Scale for Alkali and Halide Ions Established from Simulations with a Polarizable Force Field. *J. Phys. Chem. B* **2006**, *110*, 3308−3322.
(66) Warren, G. L.; Patel, S. Hydration Free Energies of Monovalent Ions in Transferable Intermolecular Potential Four Point Fluctuating Charge Water: An Assessment of Simulation Methodology and Force Field Performance and Transferability. *J. Chem. Phys.* **2007**, *127* (064509), 1−19.
(67) Warren, G. L.; Patel, S. Comparison of the Solvation Structure of Polarizable and Nonpolarizable Ions in Bulk Water and Near the Aqueous Liquid-Vapor Interface. *J. Phys. Chem. C* **2008**, *112*, 7455−7467.
(68) Warren, G. L.; Patel, S. Electrostatic Properties of Aqueous Salt Solution Interfaces: A Comparsion of Polarizable and Nonpolarizable Ion Models. *J. Phys. Chem. B* **2008**, *112*, 11679−11693.
(69) Bauer, B. A.; Ou, S.; Patel, S. Solvation Structure and Energetics of Single Ions at the Aqueous Liquid-Vapor Interface. *Chem. Phys. Lett.* **2011**, *527*, 22−26.
(70) Bauer, B. A.; Ou, S.; Patel, S. Role of Spatial Ionic Distribution on the Energetics of Hydrophobic Assembly and Properties of the Water/Hydrophobe Interface. *Phys. Chem. Chem. Phys.* **2012**, *14*, 1892−1906.
(71) Wick, C. D.; Lee, A. J.; Rick, S. W. How Intermolecular Charge Transfer Influences the Air-Water Interface. *J. Chem. Phys.* **2012**, *137* (154701), 1−9.
(72) Lee, A. J.; Rick, S. W. The Effects of Charge Transfer on the Properties of Liquid Water. *J. Chem. Phys.* **2011**, *134* (184507), 1−9.
(73) Darden, T.; York, D.; Pedersen, L. Particle Mesh Ewald: An $N \cdot \log(N)$ Method for Ewald Sums in Large Systems. *J. Chem. Phys.* **1993**, *98* (10089−10092), 1−4.
(74) Wong, K.-Y.; York, D. M. Exact Relation between Potential of Mean Force and Free-Energy Profile. *J. Chem. Theory Comput.* **2012**, *8*, 3998−4003.

(75) Zhu, F.; Hummer, G. Convergence and Error Estimation in Free Energy Calculations Using the Weighted Histogram Analysis Method. *J. Comput. Chem.* **2012**, *33*, 453−465.
(76) Flyvbjerg, H.; Petersen, H. G. Error Estimates on Averages of Correlated Data. *J. Chem. Phys.* **1989**, *91*, 461−466.
(77) Lamoureux, G.; Roux, B. Modeling Induced Polarization with Classical Drude Oscillators: Theory and Molecular Dynamics Simulation Algorithm. *J. Chem. Phys.* **2003**, *119* (3025−3039), 1−15.
(78) Ou, S.; Bauer, B. A.; Patel, S. Free Energetics of Carbon Nanotube Association in Pure and Aqueous Ionic Solutions. *J. Phys. Chem. B* **2012**, *116*, 8154−8168.
(79) Zangi, R.; Berne, B. J. Temperature Dependence of Dimerization and Dewetting of Large-Scale Hydrophobes: A Molecular Dynamics Study. *J. Phys. Chem. B* **2008**, *112*, 8634−8644.
(80) Rose, D.; Benjamin, I. Free Energy of Transfer of Hydrated Ion Clusters from Water to an Immiscible Organic Solvent. *J. Phys. Chem. B* **2009**, *113*, 9296−9303.
(81) Pershan, P. S.; Schlossman, M. *Liquid Surfaces and Interfaces: Synchrotron X-ray Methods*; Cambridge University Press: Cambridge, 2012; p 4.
(82) Willard, A. P.; Chandler, D. Instantaneous Liquid Interfaces. *J. Phys. Chem. B* **2010**, *114*, 1954−1958.
(83) Rogers, D. M.; Beck, T. L. Quasichemical and Structural Analysis of Polarizable Anion Hydration. *J. Chem. Phys.* **2010**, *132* (014505), 1−12.
(84) Ahmed, N. A.; Gokhale, D. V. Entropy Expressions and Their Estimators for Multivariated Distributions. *IEEE Trans. Inf. Theory* **1989**, *35*, 688−692.